Cylindrical Slot FSS Configuration for Beam-Switching Applications

Bin Liang, Benito Sanz-Izquierdo, Edward A. Parker, and John C. Batchelor, *Senior Member, IEEE*

***Abstract*—A novel design for a beam-switching antenna using active cylindrical slot frequency selective surface (ACSFSS) is presented. The antenna system is composed of an omnidirectional monopole antenna and the ACSFSS, which employs a new technique of switching slot arrays. The ACSFSS is made up of 12 columns with 8 slots each, dividing the cylinder by 30°. To steer the beam of the antenna the diodes are set OFF and ON, so that the radiation pattern of the antenna is determined by the number of OFF state columns. To estimate the general dimension of the cylindrical FSS, an equivalent metallic reflector is introduced and optimized, and then parametric studies for the unit cell dimensions are discussed. The fabricated prototype works within the WLAN band, centered around 2.45 GHz, and can agilely select either a narrow-beam or wide-beam operating mode. Simulation and measurements confirm the operation of the ACSFSS antenna, with good matching and gain observed. In particular, the narrow-beam mode −3 dB beamwidth is 47° which offers enhanced angular resolution compared with other reported beam-sweeping work.**

***Index Terms*—Beam-sweeping, beam-switching, frequency selective surfaces (FSS), slot arrays.**

I. Introduction

AS A COMMON technology nowadays, most wireless local area networks (WLAN) use the same frequency band in the narrow range lying between 2.4–2.5 GHz. Consequently, although linking many systems together can easily result in better communication and compatibility, it also leads to serious problems of interference. In WLAN systems, interference results in not only serious issues such as lower capacity, but also a prominent decrease in connection speeds and sometimes lack of connectivity due to the unavailability of free access channels.

As a solution to the above demerits, beam-switching in WLAN systems can bring a significant decrease in the rate of interfering signals and improvement of capacity, by steering the antenna beams away from co-channel access points [1]–[4]. There are various methods for designing beam-switching antennas, such as conventional phased antenna array but they are either complicated or high cost.

Recently, active frequency selective surfaces (AFSS) have drawn significant interest from researchers investigating beam-steering techniques for antenna applications [5]–[14]. Frequency selective surfaces (FSS) are periodic structures which serve as a filter to electromagnetic waves [15], [16]. They can be either transmitting or reflecting in operating frequency bands, determined by the design of unit cells. By employing active devices like PIN and varactor diodes, AFSS can achieve high level of control over electromagnetic wave propagation, such as switching the FSS between transmitting and reflecting modes. In order to realize the switching between omnidirectional and directional radiation patterns, as well as the capacity of beam-sweeping, active cylindrical FSS (ACFSS) with multiple-layer [5]–[7] or single-layer [5], [6] metallic wires have been explored, and active cylindrical patch FSS (ACPFSS) have been studied and reported recently [8]–[11]. In [8]–[11], omnidirectional antennas are placed at the center of the ACPFSS, and the 360° azimuth plane is divided into several sectors. By switching the diodes states, sectors of the ACPFSS cylinder can be made either transparent or opaque in the operating frequency band, so that the antenna beam can be steered in required patterns and directions. According to the reported results, the designs have successfully achieved omni-directional-to-directional switching as well as beam-sweeping, with acceptable gains. Nevertheless, since the basic unit cell of the FSS in these designs employed discontinuous conducting patches connected by pin diodes, the FSS could not provide a completely transparent level for the incident waves at the desired frequency when diodes were activated. As a result, this considerably degrades the performance of the radiation pattern, as mentioned in [11]. Through designing a hybrid patch unit cell (HPUC), the transparency level was improved in [11] and it presented a band-pass characteristic at the desired frequency when diodes were ON. However, when the diodes were OFF, the FSS offered a transmission level of only −7 dB. The corresponding reflectivity level was inadequate, and brought considerable energy loss when the FSS served as a reflector. As an alternative, the slot FSS is the Babinet counterpart of the conducting patch FSS, acting as a band-pass filter, which can provide sufficient transparency level. When the diodes are activated, the AFSS performs as a reflector to reflect signals by a notable improved level. Although band-pass AFSS has been studied for beam-steering applications [17], it has not been previously reported as part of the ACFSS.

In this paper, a new design of beam-switching antenna system is proposed, which uses the active cylindrical slot

Manuscript received July 10, 2013; revised August 11, 2014; accepted October 12, 2014. Date of publication November 05, 2014; date of current version December 31, 2014. This work was supported by the China Scholarship Council (CSC).

B. Liang is with the Microwave Engineering Laboratory, Beihang University, Beijing 100191, China, and also with the School of Engineering and Digital Arts, University of Kent, Canterbury CT2 7NT, U.K. (e-mail: bl213@kent.ac.uk).

B. Sanz-Izquierdo, E. A. Parker, and J. C. Batchelor are with the School of Engineering and Digital Arts, University of Kent, Canterbury CT2 7NT, U.K. (e-mail: b.sanz@kent.ac.uk).

Color versions of one or more of the figures in this paper are available online at http://ieeexplore.ieee.org.

Digital Object Identifier 10.1109/TAP.2014.2367534

This work is licensed under a Creative Commons Attribution 3.0 License. For more information, see http://creativecommons.org/licenses/by/3.0/

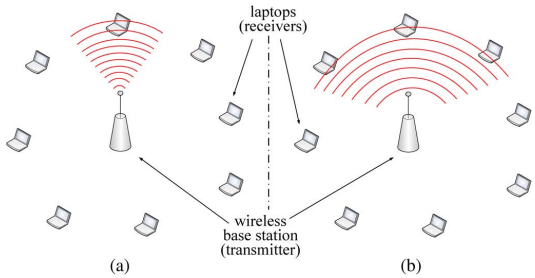

Fig. 1. Schematic diagram of the beam coverage in different applications: (a) application of narrow beamwidth and (b) application of wide beamwidth.

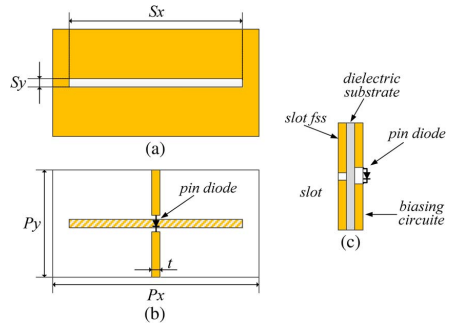

Fig. 2. Unit cell of active frequency selective slot array: (a) front view with slot, (b) rear view with biasing circuit, and (c) side view of biasing configuration.

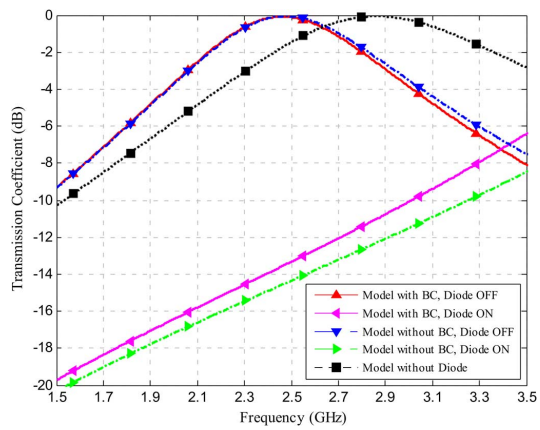

Fig. 3. Simulated transmission coefficients of the FSS unit cell.

FSS (ACSFSS) to realize high-level control of the beam. The radiation source is an omnidirectional monopole which is surrounded by the ACSFSS. The cylindrical FSS is composed of twelve columns each with eight unit cells containing horizontal slots. A double-sided biasing technique [18] is adopted here, which effectively supplies separate DC-biasing for the diodes in the columns of the ACSFSS. The cylinder surface can be divided into two areas of biased adjacent columns, where the diodes in one surface are ON, while the rest in the other surface are OFF. The area with ON-state diodes serves as a reflector in the operating frequency band, whereas the other surface with OFF-state diodes operates as a band-pass FSS at the resonant frequency. As a consequence, the omnidirectional radiation pattern of the monopole can be converted into a directional one. Owing to the axial symmetry, the directional pattern can be swept in the entire 360° azimuth plane with different beam shapes, determined by the number of columns with OFF-state diodes. As is shown in Fig. 1, the beam coverage can be adjusted depending on the number of receivers, which can be used in different applications. From the simulated and measured results, it can be seen that acceptable matching and gain are obtained in different switching states. The proposed ACSFSS antenna system can be used in WLAN systems in the range of 2.4–2.5 GHz.

The rest of this paper is organized as follows. In Section II, unit cell design of the band-pass FSS is presented, as well as the introduction of the biasing technique. The effect of the pin diode and biasing circuit is also provided. In Section III, the mechanism and principle of the ACSFSS antenna design is presented, including the antenna diagram and overall dimensions. In order to show the effect of the unit cell dimensions on the radiating characteristics of the antenna, parametric studies of the equivalent metallic reflector and the ACSFSS antenna are shown in Section IV, including some discussions as well. In Section V, experimental results of the fabricated prototype are provided and discussed. Finally, the paper is concluded in Section VI.

II. Unit Cell Design

The transmission responses of reconfigurable band-pass FSS were discussed in [12], [14], [18]. By employing pin diodes, the FSS can be switched between transmitting and reflecting states. Fig. 2 illustrates the unit cell of an active FSS consisting of a double-sided structure, in which the biasing circuit is isolated from the passive FSS conducting elements [18]. The structure was printed on flexible polyester substrate of 0.05 mm thickness with metal cladding on its two sides. The FSS with the slots were on the front while pin diodes were placed on the biasing circuit at the back. The dimensions of the unit cell were: $Px = 57$ mm, $Py = 25$ mm, $Sx = 55$ mm, $Sy = 0.5$ mm, and $t = 2$ mm. The relative permittivity of the substrate is approximately 3. The structure was simulated in CST Microwave Studio, in which the diode is modeled as *RLC* serial lumped elements. In the ON-state, the diode is equal to a forward resistance with $Rs = 2.1\,\Omega$, while in the OFF-state at 0 V the equivalent model is a capacitance of $Cs = 0.2$ pF. It should be pointed out that several sets of dimensions can result in a resonant frequency of about 2.45 GHz, but the specific set of values here have been optimized for the ACSFSS. The optimization procedure is described in the following sections.

The transmission coefficients of the unit cell in both ON and OFF states are presented in Fig. 3. The solid lines are the simulation results of the model with biasing circuit (BC), while the dotted-dashed lines refer to the model with lumped element directly added to the slot without the BC. The dotted line corresponds to the model without diodes or the BC. All three models have the same dimensions. As can be seen from the figure, the diode decreases the resonant frequency of the band-pass FSS significantly, while the BC has a minor effect on the transmission curves. When the diode is OFF, the AFSS shows wideband transmission centered at 2.45 GHz. When the diode is ON, the FSS offers transmission levels below -13 dB at the WLAN band.

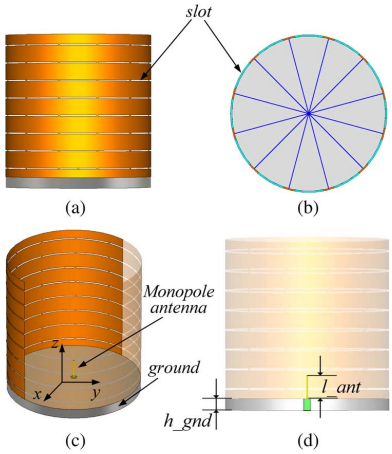

Fig. 4. ACSFSS antenna schematic: (a) side view, (b) top view, (c) perspective, and (d) close-up of the monopole.

III. Antenna Schematic and Mechanism

The schematic of the antenna is presented in Fig. 4. For clarity, half of the cylindrical FSS in the perspective view has been made transparent. The radiating source is composed of a monopole antenna in the center with a round metallic plate as ground. As a standard monopole, the antenna radiates an omnidirectional pattern in the azimuth plane (x–y plane) and a directional pattern in the elevation planes. The ACSFSS, which has the same radius as the ground plate, encircles the monopole. The ACSFSS has twelve columns each subtending an angle of 30° at the circle center. Each vertical column contains eight unit cells with horizontal slots. Consequently, eight pin diodes are required per column. For simplicity, the diodes and biasing circuits are not shown in Fig. 4.

The operation mechanism of the ACSFSS antenna is as follows. The 12 columns are divided into 2 sectors, of which all the diodes in one sector are set OFF while those in the other sector are set ON. The sector with diodes OFF allows transmission from the antenna, while the sector with diodes ON acts as a metallic reflector. By switching the diodes in each column, not only can the function of beam-sweeping in the entire 360° of the azimuth plane be achieved, but the beamwidth and signal coverage can be adjusted.

It is worthwhile pointing out that the transmission and reflection coefficients of the unit cell design are obtained on the basis of Floquet's theory for an infinite planar periodic structure, so that the curved cylindrical FSS may change the electromagnetic response. The factors impacting the performance include the structure of the unit cell, the radius of the curvature and the incident angle of the electromagnetic wave [19]. Nevertheless, due to the symmetry of the proposed ACSFSS-antenna system, a small discrepancy of the electromagnetic performance between the infinite planar FSS and cylindrical FSS can be expected as long as their tangential dimensions are the same [11]. Therefore, the radius of the cylinder can be calculated as

$$R_{\mathrm{FSS}} = \frac{12 \cdot Px}{2\pi}. \tag{1}$$

TABLE I
Final Dimensions of the ACSFSS

Parameters	Px	Sx	Py	Sy
Value	57mm	55 mm	25 mm	0.5 mm
Parameters	h_{gnd}	R_{gnd}	l_{ant}	r_{ant}
Value	15mm	108.86 mm	29.1mm	1 mm

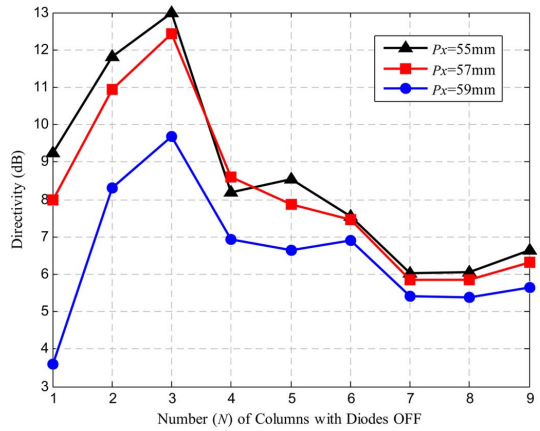

Fig. 5. Effect of N and Px on directivity of the metallic reflector.

The dimensions of the ACSFSS antenna listed in Table I were achieved by comprehensive parametric studies to optimize the radiation characteristics, which will be presented in the following section. In the table, h_{gnd} is the thickness of the ground plate, R_{gnd} is the radius of the ground as well as the cylindrical FSS, while l_{ant} and r_{ant} are the length and radius of the monopole above the ground, respectively.

IV. Parametric Studies and Discussions

A. Cylindrical Reflector Antenna Optimization

It is well known that the resonant frequency of the band-pass FSS shifts as the length of slot and periodicity change. Therefore, there are many sets of the combinations of Sx and Px that can result in the target resonant frequency of 2.45 GHz. Since the parameter R_{FSS} is the major factor that determines the overall dimension of the cylinder and ground plate, which mainly influences the radiation performance of the antenna, it is necessary to firstly optimize the horizontal tangential periodicity Px which defines R_{FSS} by (1). For simplification, the parametric studies of Px were developed by using an equivalent metallic reflector in the columns switched to reflecting state.

The size of the aperture of the equivalent reflector can be calculated from the corresponding number of columns in the OFF-state (N). As shown in Fig. 5, the largest directivity is obtained at $N = 3$, regardless of the value of Px. The directivity is highest at $Px = 55$ mm but $|S_{11}|$ is over -5 dB in the 2.4 to 2.5 GHz band (see Fig. 6). In addition, the resonant frequency increases dramatically with the decrease of Px and N, and $|S_{11}|$ is degraded at the desired band. The larger Px is, the better the $|S_{11}|$, but the lower the directivity. Therefore, as long as an acceptable level of $|S_{11}|$ is achieved for a small value of N, matching will be acceptable at larger N.

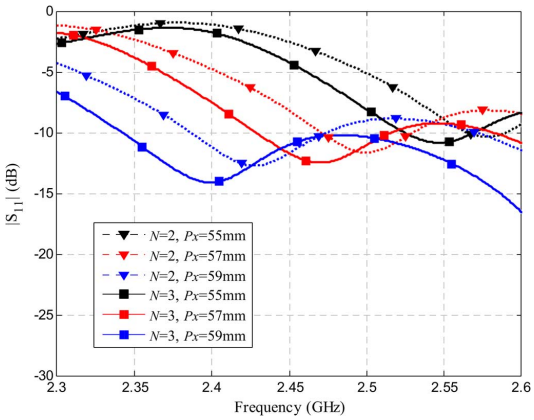

Fig. 6. Effect of N and Px on $|S_{11}|$ of the metallic reflector.

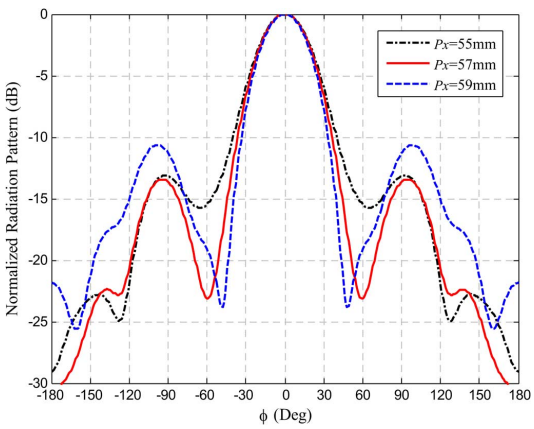

Fig. 7. Effect of Px on radiation pattern of the metallic reflector $N = 3$.

Fig. 7 illustrates the H-plane radiation pattern for different levels of Px, in which the x-axis label φ denotes the azimuth angle. The lowest side/back-lobes are found at $Px = 57$ mm. Considering all the radiation characteristics (see Figs. 5 and 7) as well the matching of the antenna (see Fig. 6), the optimal value of Px for our applications is 57 mm.

B. ACSFSS Antenna

To evaluate the radiation performance of the ACSFSS antenna, simulated results of the full structure with the slots and diodes are discussed in this section. The very thin polyester substrate and the BCs were found to contribute little to the antenna characteristics other than less than 1 dB loss in the H-plane gain, and a slight difference in the direction of the main lobe in the E-plane. However, the meshing process and the simulation time were significantly increased, making the parametric studies time-consuming and impractical. Therefore, the thin substrate and the BC were not taken into account in the following simulations, but they can be regarded as a guide to the experiment and one of the explanations of the gap between simulated and measured gains.

As with the simplified model, the best narrow-beam pattern with the highest realized gain is obtained in the state of $N = 3$, and the normalized radiation pattern is presented in Fig. 8. It can be observed that the half-power beamwidth and side/back-lobe agree with those of the equivalent metallic reflector simulation

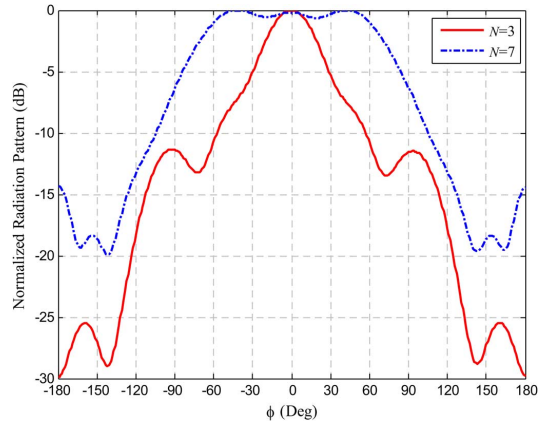

Fig. 8. Two modes of radiation pattern.

shown as the red line in Fig. 7, while the -10 dB beamwidth is notably wider probably due to the effects of FSS and diodes.

It was found in the simulation of the ACSFSS antenna that the state $N = 7$ produces a wide-beam radiation pattern (see Fig. 8), which can be used in applications requiring wide signal coverage such as the one illustrated in Fig. 1(b). However, since the narrow-beam radiation pattern is the most common case studied in previous research on beam-sweeping antennas using FSS [8]–[11], the parametric studies in this section are mainly focused in the case when $N = 3$.

Besides Px, other dimensions of the unit cell are Py, Sx, and Sy, which control the transmission (and reflection) response of the planar AFSS (as shown in Fig. 9), and hence also influence the radiating characteristics of the ACSFSS. Note that in Fig. 9 there are different axis labels for the diodes in OFF and ON states. On one hand, in terms of the reflecting mode (the diodes are ON), the transmission levels are all less than -13 dB at 2.45 GHz whatever the values of Py and Sx. The radiating characteristics are relatively insensitive to them. Nevertheless, when $Sy = 2.0$ mm the transmission level is above -9 dB as shown in Fig. 9(b), which means some energy leak from the reflective part of the cylinder and causes almost 10 dB increase of the back-lobe in the radiation pattern, as shown in Fig. 10(a). On the other hand, in terms of the transmitting mode (the diodes are OFF), as the dimensions of these parameters increase, the transmission peak shifts towards lower frequencies, as presented in Fig. 9. This means the transmitting part of the cylinder becomes more reflective at other frequencies and the antenna matching is degraded. As a result, the resonant frequency of the antenna matching is correspondingly reduced. It should be noted that although the transmission curves in Fig. 9(a) are at minor levels (less than -0.3 dB over 2.4–2.5GHz), the effect on $|S_{11}|$ is still notable, owing to the increasing height of the equivalent reflector as Py increases. Since the tendencies of $|S_{11}|$ affected by these parameters are similar to those in Fig. 6, the graphs are not presented here for brevity.

As the effects of Py and Sy on the realized gain around 2.45 GHz are small, graphs have not been included as well, but the corresponding results are reported here. Specifically, differences of the realized gain caused by varying Py from 20 to 30 mm are less than 0.5 dB, while those caused by Sy from 0.2

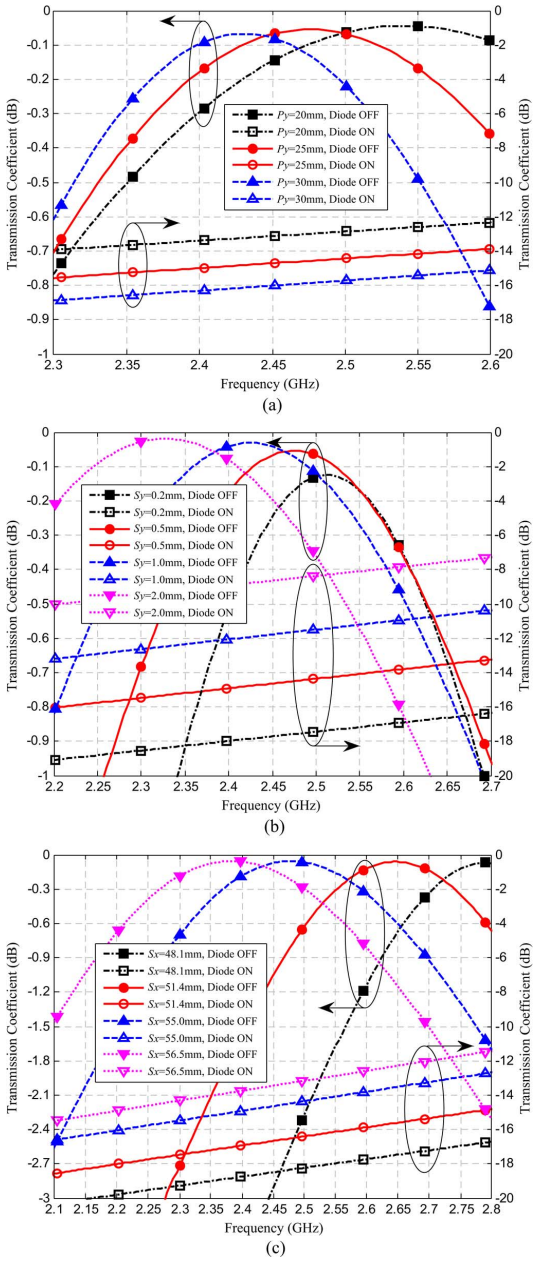

Fig. 9. Parametric study of the transmission coefficient of the planar AFSS by changing (a) Py, (b) Sy, and (c) Sx.

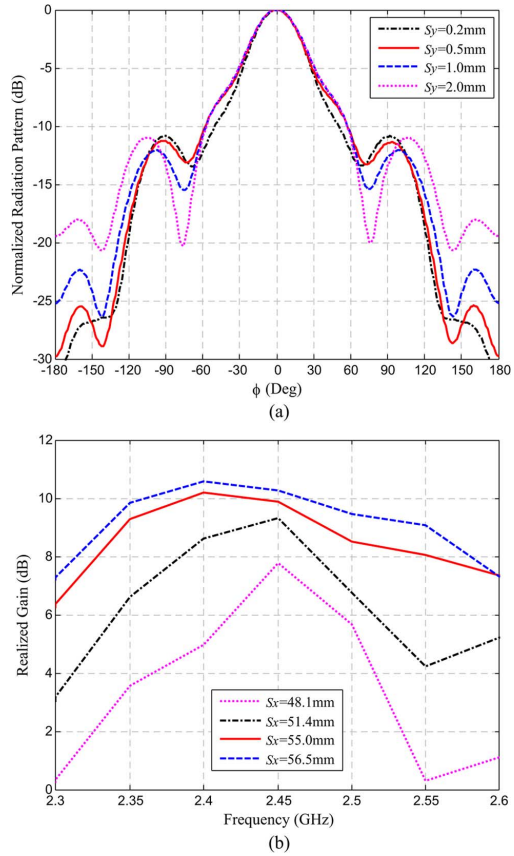

Fig. 10. Parametric study of antenna parameters in the state of $N = 3$. (a) Radiation pattern for different values of Sy. (b) Realized gain for different values of Sx.

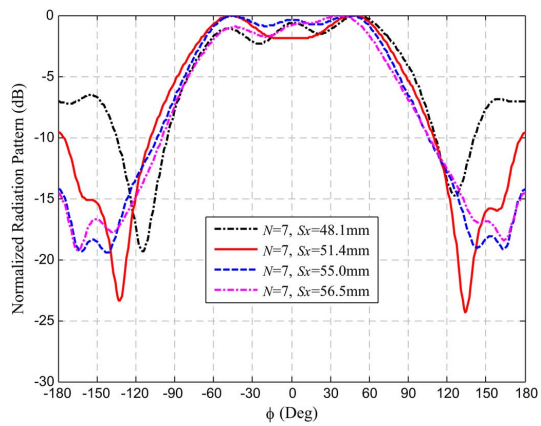

Fig. 11. Parametric study of radiation patterns for various Sx values in the state of wide-beam mode.

to 1.0 mm are less than 0.3 dB, but $Sy = 2.0$ mm leads to a significant 1.2 dB decline of the realized gain, at the operating frequency 2.45 GHz, which is also due to the low reflection level as aforementioned. In contrast, the effect of Sx on the realized gain is significant, as presented in Fig. 10(b). The difference between the maximum and minimum value at 2.45 GHz is 2.5 dB, while it is 1.7 dB if the mismatch effect is not counted. The reduced gain is mainly due to the considerable transmission loss (3 dB) when $Sx \approx 48$ mm, hence the EM wave energy is notably degraded by the transmitting window. Although the results for $Sx = 56.5$ mm are slightly better than those of $Sx = 55$ mm in terms of the radiation pattern and realized gain, the $|S_{11}|$ at $Sx = 55$ mm is optimum in the range of 2.4–2.5 GHz.

In addition, with regard to the case when $N = 7$, although the tendency of realized gain in terms of Sx is similar to that of $N = 3$, the radiation pattern has minimal main-lobe ripple when $Sx = 55$ mm, as shown in Fig. 11. Therefore, to achieve the most comprehensive tradeoff in terms of all radiation characteristics in the two available states, 55 mm is believed to be the optimal value of Sx.

C. Comparison With the ACPFSS

In order to verify the advantage of the ACSFSS in beam-switching, the hybrid patch unit cell (HPUC) was employed in

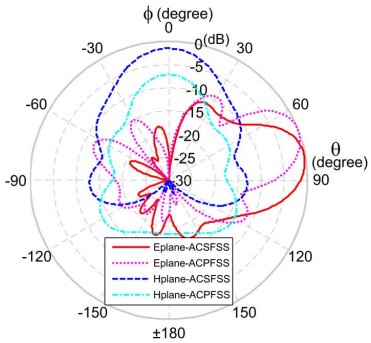

Fig. 12. Comparison between the radiation patterns of ACSFSS and ACPFSS.

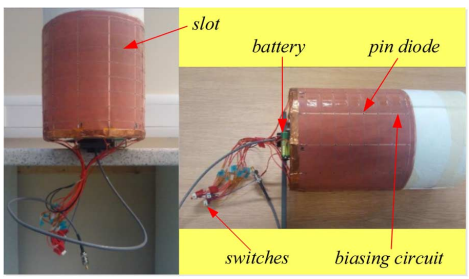

Fig. 13. Photograph of the fabricated ACSFSS antenna prototype.

the cylindrical FSS by replacing the slot unit cell as a comparison. The structure and parameters of the HPUC can be referred to [11]. Since the two cylinders with different unit cells should be of the same radius and height, Px and Py of the HPUC were slightly adjusted to 28.5 and 50 mm, respectively. Through optimizing other dimensions, the adjusted HPUC could provide transparency and reflection levels around 2.45 GHz. Consequently, the whole ACPFSS was composed of 24 columns by 4 rows of HPUCs, and 6 columns of the diodes were set ON to make the antenna work in the same directional mode as that of the ACSFSS when $N = 3$. The simulated E- and H-plane radiation patterns at 2.45 GHz of the two structures are presented in Fig. 12. In order to show clearly the gain reduction, the four patterns are normalized by the maximum value of them. It can be seen that in terms of the E-plane pattern, the back-lobe of the ACPFSS pattern is notably higher than that of the ACSFSS pattern. This is due to the low reflection level, which also displaces the main lobe. As a result, a reduction of more than 5 dB is caused when $\theta = 90°$, correspondingly the gain of the H-plane pattern is significantly reduced.

V. Fabrication and Measurement Results

To validate the performance of the proposed antenna, a prototype was fabricated and measured. The monopole antenna used was the commercial antenna Cushcraft SM2403M, which operates over 2.4–2.5 GHz frequency range. A planar FSS was firstly fabricated, which consisted of 12×8 slot unit cells of the dimensions in Table I. Twelve parallel biasing lines with eight diodes each were etched in the rear side, and the slots on the front. At the end of each bias line, a resistor of 1 kΩ was used to limit the current of the diodes. As in [14], [18], BAR64-02 silicon pin diodes were employed. As shown in Fig. 13, the planar

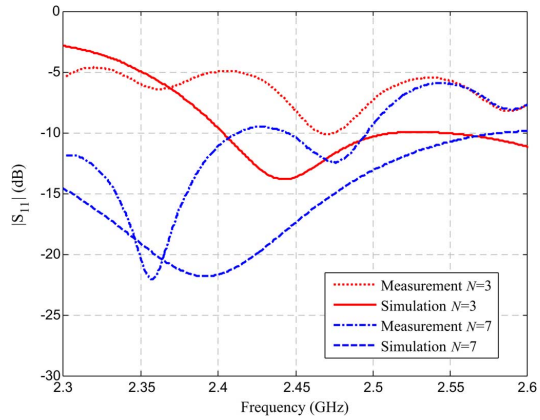

Fig. 14. Simulation and measurement results of $|S_{11}|$.

FSS was wrapped onto a purposely made cylindrical polystyrene foam ($\varepsilon_r = 1.04$) [20], and a centered aperture was created at the bottom of the cylinder to accommodate the monopole antenna.

For the measurements, DC voltage was supplied by an external 1604 G GP Greencell battery of 9 V. Twelve small switches were used to connect the battery and the biasing wires. When a switch was OFF, the DC voltage of the corresponding column was zero, and all eight diodes in the column were OFF. When a switch was ON, a DC voltage of about 6 V was found at the end of the eight diodes in the column, and the diodes were in the ON-state.

The measured $|S_{11}|$ of the antenna in the $N = 3$ and 7 states are shown in Fig. 14, together with simulated results. According to measurement, the ACSFSS antenna had reflection coefficients of less than -6 dB in the desired operating band centered around 2.45 GHz. As expected, the more columns of diodes OFF, the better the matching obtained. The deviations between simulation and measurement results were caused by the following factors. First, the polyester substrate of 0.05 mm thickness and biasing circuits were not considered in simulation, since extremely small dimensions could greatly increase the amount of mesh cells and computational requirements. Second, the cable and the adapter were not included in the simulation model, being replaced by a waveguide port in CST. Third, some fabrication and measurement errors might exist.

The radiation patterns were measured in our anechoic chamber, and the results at 2.40, 2.45, and 2.50 GHz are shown in Figs. 15 and 16, together with the simulation results at 2.45 GHz. In the state of $N = 3$, the -3 dB beamwidth at 2.45 GHz in the azimuth plane (H-plane) was 47°, while that in the elevation plane (E-plane) was 27°. It is worthwhile pointing out that, the beamwidth in the azimuth plane obtained in this design was much smaller than those mentioned in [9] and [10], which were 60° and 70°, respectively. Consequently, a higher angular resolution in beam-sweeping application was obtained. In the state of $N = 7$, a wide-beam radiation pattern was realized, of which the -3 dB beamwidth was 145° in the H-plane with a maximum fluctuation of 1.7 dB in the main beam, whereas in the E-plane the -3 dB beamwidth was 35°.

It can be observed that the H-plane patterns were not completely symmetrical with respect to zero degree as expected,

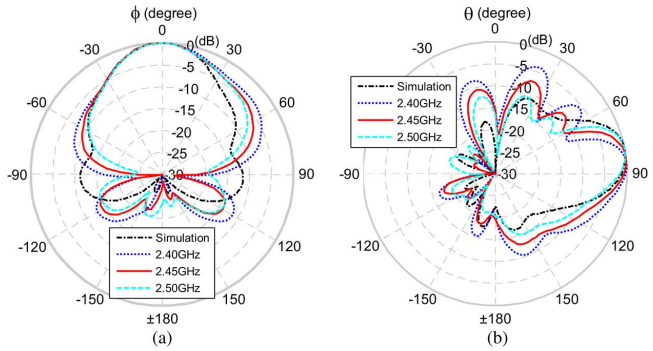

Fig. 15. Measured radiation patterns in narrow-beam mode (N=3). (a) H-plane. (b) E-plane.

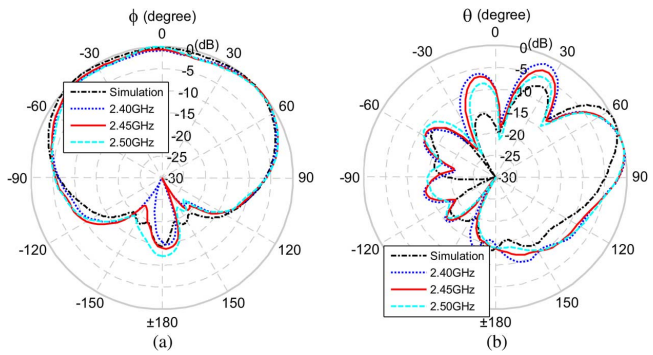

Fig. 16. Measured radiation patterns in wide-beam mode ($N = 7$). (a) H-plane. (b) E-plane.

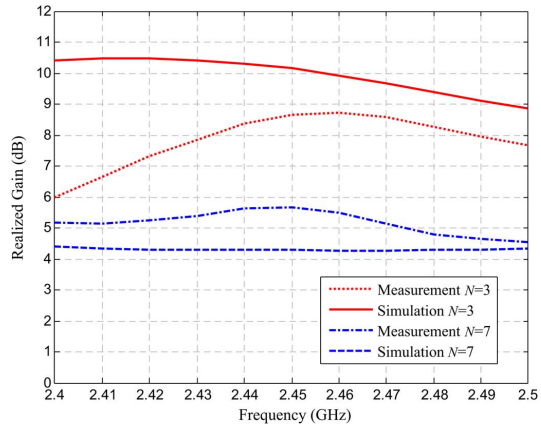

Fig. 17. Simulation and measurement results: realized gain in H-plane.

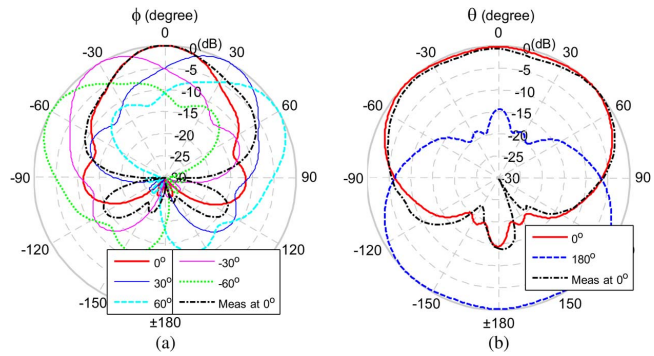

Fig. 18. Beam-sweeping characteristic of the antenna at 2.45 GHz: (a) narrow-beam mode and (b) wide-beam mode.

which is believed to be caused by some fabrication errors, such as misalignments during the placement of the FSS screen on the cylindrical polystyrene foam. With regard to the E-plane patterns, the main-lobe direction was tilted from the horizontal plane by 10° in simulation while 6° in measurement when $N = 3$, whereas it was tilted by 25° in simulation while 15° in measurement when $N = 7$. It is noticed that the measurement results performed better than simulations in terms of the tilt level of the E-plane pattern, as the cable and adapter used in the measurements were not considered in the simulations. As a result, reductions of only 0.7 dB in the narrow-beam mode and 2.0 dB in the wide-beam mode of the measured gain were caused by the tilted pattern. The beam sweeping characteristics of the antenna are shown in Fig. 18.

The gain of the ACSFSS antenna was measured by the comparison method, and the results together with simulation are shown in Fig. 17. It can be seen that in the narrow-beam mode, the realized gain is more than 6 dB in the entire operating band and more than 8 dB around the center (2.45 GHz). In addition, it is observed that in the wide-beam mode, the measured gain is larger than simulated. This is because of a shift of the maximal gain direction in the elevation plane, which makes the measured value at $\theta = 90°$ larger than that of the simulated one, as shown in Fig. 16(b). Besides the very thin substrate and the biasing circuit (BC) neglected in simulation, together with fabrication and measurement errors, the actual physical characteristics of the diode enclosure could be another reason for the differences between the simulated and measured gains.

VI. Conclusion

In this paper, a cylindrical active FSS antenna using slot unit cells is proposed for beam-switching application. The cylindrical FSS employs a double-sided biasing technique to supply voltage to pin diodes, which are employed to switch the sectors of the FSS between transparent and opaque states. Through switching the diodes ON and OFF, different radiation patterns can be obtained. A model based on unslotted reflectors can be used effectively to optimize the radius of the cylinder to obtain the radiation characteristics of the ACSFSS antenna. A full model of the ACSFSS antenna using diodes directly connected to the slots can demonstrate the effect of the other important parameters on $|S_{11}|$ and the radiation patterns. Simulations and measurement of the prototype verifies that two main modes of radiation pattern can be realized: the narrow-beam, and the wide-beam. The measured reflection coefficients of the antenna in both modes were acceptable at 2.45 GHz WLAN band. The measured H-plane gain was 8.7 dB at the central frequency in the most commonly used narrow-beam mode. In addition, the beamwidth of the mode is notably narrower than those reported earlier [8]–[11], so that the angular resolution can be enhanced in beam-sweeping applications. In conclusion, the multi-mode ACSFSS antenna can be used agilely for WLAN communication systems. Compared with patch based techniques [8]–[11], the ACSFSS described here has the potential to achieve more advanced beam steering techniques using already published AFSS configurations [14], [18]. This will be studied in the future.

REFERENCES

[1] M. Chryssomallis, "Smart antennas," *IEEE Antennas Propag. Mag.*, vol. 42, pp. 129–136, 2000.

[2] M.-I. Lai, T.-Y. Wu, J.-C. Hsieh, C.-H. Wang, and S.-K. Jeng, "Compact switched-beam antenna employing a four-element slot antenna array for digital home applications," *IEEE Trans. Antennas Propag.*, vol. 56, no. 9, pp. 2929–2936, Sep. 2008.

[3] A. Alexiou and M. Haardt, "Smart antenna technologies for future wireless systems: Trends and challenges," *IEEE Commun. Mag.*, vol. 42, no. 9, pp. 90–97, Sep. 2004.

[4] G. Cerri, R. De Leo, V. M. Primiani, C. Monteverde, and P. Russo, "Design and prototyping of a switching beam disc antenna for wideband communications," *IEEE Trans. Antennas Propag.*, vol. 54, no. 12, pp. 3721–3726, Dec. 2006.

[5] H. Boutayeb, T. Brillat, J. Daniel, F. Gadot, P. Garel, A. De Lustrac, K. Mahdjoubi, P. Ratajczak, and A.-C. Tarot, "A reconfigurable electromagnetic bandgap structure for a beam steering base station antenna," presented at the 27th ESA Antenna Technol. Workshop Innovative Periodic Antennas, Santiago de Compostela, Spain, Mar. 2004.

[6] H. Boutayeb, A.-C. Tarot, and K. Mahdjoubi, "Focusing characteristics of a metallic cylindrical electromagnetic band gap structure with defects," *Progr. Electromagn. Res.*, vol. 66, pp. 89–103, 2006.

[7] H. Boutayeb, T. A. Denidni, K. Mahdjoubi, A.-C. Tarot, A.-R. Sebak, and L. Talbi, "Analysis and design of a cylindrical EBG-based directive antenna," *IEEE Trans. Antennas Propag.*, vol. 54, no. 1, pp. 211–219, Jan. 2006.

[8] M. N. Jazi and T. A. Denidni, "Frequency selective surfaces and their applications for nimble-radiation pattern antennas," *IEEE Trans. Antennas Propag.*, vol. 58, no. 7, pp. 2227–2237, Jul. 2010.

[9] A. Edalati and T. A. Denidni, "High-gain reconfigurable sectoral antenna using an active cylindrical FSS structure," *IEEE Trans. Antennas Propag.*, vol. 59, no. 7, pp. 2464–2472, Jul. 2011.

[10] A. Edalati and T. Denidni, "Frequency selective surfaces for beam-switching applications," *IEEE Trans. Antennas Propag.*, vol. 61, no. 1, pp. 195–200, Jan. 2013.

[11] M. Niroo Jazi and T. A. Denidni, "Electronically sweeping-beam antenna using a new cylindrical frequency selective surface," *IEEE Trans. Antennas Propag.*, vol. 61, no. 2, pp. 666–676, Feb. 2013.

[12] G. I. Kiani, K. L. Ford, L. G. Olsson, K. P. Esselle, and C. J. Panagamuwa, "Switchable frequency selective surface for reconfigurable electromagnetic architecture of buildings," *IEEE Trans. Antennas Propag.*, vol. 58, no. 2, pp. 581–584, Feb. 2010.

[13] I.-Y. Tarn and S.-J. Chung, "A novel pattern diversity reflector antenna using reconfigurable frequency selective reflectors," *IEEE Trans. Antennas Propag.*, vol. 57, no. 10, pt. 2, pp. 3035–3042, Oct. 2009.

[14] B. Sanz-Izquierdo, E. A. Parker, and J. C. Batchelor, "Dual-band tunable screen using complementary split ring resonators," *IEEE Trans. Antennas Propag.*, vol. 58, no. 11, pp. 3761–3765, Nov. 2010.

[15] B. A. Munk, *Frequency Selective Surfaces: Theory and Design*. New York, NY, USA: Wiley, 2000.

[16] R. Mittra, C. H. Chan, and T. Cwik, "Techniques for analyzing frequency selective surfaces-a review," *Proc. IEEE*, vol. 76, no. 12, pp. 1593–1615, Dec. 1988.

[17] L. Boccia, I. Russo, G. Amendola, and G. Di Massa, "Tunable frequency-selective surfaces for beam-steering applications," *Electron. Lett.*, vol. 45, pp. 1213–1215, 2009.

[18] B. Sanz-Izquierdo, E. A. Parker, J.-B. Robertson, and J. C. Batchelor, "Tuning technique for active FSS arrays," *Electron. Lett.*, vol. 45, pp. 1107–1109, 2009.

[19] B. Philips, E. A. Parker, and R. J. Langley, "Finite curved frequency selective surfaces," *Electron. Lett.*, vol. 29, pp. 882–883, 1993.

[20] P. S. Taylor, E. A. Parker, and J. C. Batchelor, "An active annular ring frequency selective surface," *IEEE Trans. Antennas Propag.*, vol. 59, no. 9, pp. 3265–3271, Sep. 2011.

Bin Liang received the B.Sc. degrees in electronic and information engineering from Beihang University [Beijing University of Aeronautics and Astronautics (BUAA)], Beijing, China, in 2008. He is currently pursuing the joint Ph.D. degree from Beihang University and the University of Kent, Kent, U.K.

Since 2012, he has been a Ph.D. student visitor to the University of Kent, U.K., funded by the China Scholarship Council (CSC). His research interests include frequency selective surfaces, electromagnetic band-gap structures and computational electromagnetic.

Benito Sanz-Izquierdo received the B.Sc. degree from the University of Las Palmas de Gran Canaria, Las Palmas, Spain, and the M.Sc. and Ph.D. degrees from the University of Kent, Kent, U.K., in 2002 and 2007, respectively.

From 2003 to 2012, he was a Research Associate with the School of Engineering and Digital Arts, University of Kent, and in 2013, became a lecturer in electronic systems. In 2012, he spent some time working for Harada Industries Ltd., where he developed novel antennas for the automotive industry. His research interests include multiband antennas, wearable microwave devices, substrate integrated waveguides components, electromagnetic band-gap structures, and frequency selective surfaces.

Edward (Ted) A. Parker received the M.A. degree in physics and the Ph.D. degree in radio astronomy from Cambridge University (St. Catharine's College), Cambridge, U.K.

He was appointed Reader at the University of Kent in 1977, and since 1987, he has been Professor of Radio Communications, now Professor Emeritus. He established the Antennas Group, Electronics Laboratory, University of Kent, Kent, U.K. The early work of that group focused on reflector antenna design, later on frequency selective surfaces and patch antennas. He is a member of the IET. One of his interests is the study and overhaul of antique clocks.

John C. Batchelor (S'93–M'95–SM'07) received the B.Sc. and Ph.D. degrees from the University of Kent, Canterbury, U.K., in 1991 and 1995, respectively.

From 1994 to 1996, he was a Research Assistant with the Electronics Department, University of Kent, and in 1997, became a Lecturer of electronic engineering. He now leads the Antennas Group, University of Kent, and is a Reader in antenna technology. His current research interests include UHF RFID tag design, passive sensing, body-centric antennas, printed antennas, compact multiband antennas, electromagnetic bandgap structures, and long-wavelength FSS (frequency-selective surfaces).